Longwave estimation of cloud fraction using machine learning

Tina Andriantsalama, Beatrice Morel, Chao Tang, Remy Ineza Mugenga

April 20, 2022

Contents

1 Data and methods **3**
1.1 Datasets . . . 3
1.1.1 BSRN Reunion Moufia . . . 3
1.1.2 Longwave from Clouds and the Earth's Radiant Energy System (CERES) . . . 5
1.1.3 Cloud fraction - longwave . . . 6
1.1.4 Machine learning methods . . . 8
1.1.5 XGBoost model . . . 8
1.1.6 Artificial Neural Network . . . 8
1.1.7 Learning curve for diagnosing model . . . 9

2 Results and discussions **9**
2.1 Estimation with XGBoost . . . 9
2.2 Estimation with XGBoost . . . 12

Abstract

Many studies have shown that knowledge about the cloud fraction is a necessity for a numerical weather study and prediction model (Heidinger and Cox 1996). This paper deal for estimating cloud fraction with data from BSRN Reunion station using XGBoost machine learning model and a sequential artificial neural network. First, we did data validation, especially for longwave ground measurement, data were compared with data from CERES. The results about RMSE, MAE and correlation coefficient obtained from the comparison is very satisfactory. Secondly, the results about cloud fraction estimation with the model XGBoost and the model ANN are also very satisfactory. Score 92.21 % for XGBoost and 91.78 % for the model neural network. These are a good score according to the results mentioned in Han et al. 2019, Ma, Fang, and Ji 2020 and Dhakal, Gautam, and Bhattarai 2020. After features engineering several tests were released and we get many interesting results. And we conclude that pressure is note necessary for the model, it makes the model more complex. We proposed also to add aerosol as a feature. The link between cloud fraction and aerosol (Gryspeerdt, Quaas, and Bellouin 2016) can be important for the model and to improve estimation's results.

Keywords

Introduction

Even though clouds play a key role in the Earth's radiation budget, and its representation in Numerical Weather Prediction (NWP) models still has a long way to go (Heidinger and Cox 1996). The current uncertainties lie from misrepresentation of brokenness (inhomogeneity) of clouds in atmospheric radiative transfer calculations, which has been studied over 20 years for solar radiation in general and longwave radiation in particular (Aida 1977, Ellingson 1982). In addition to emissions, cloud brokenness effects to longwave radiation consider the side face shading of the broken cloud blocks. Estimation of the cloud brokenness has been using different approximation methods, which requires a significant computational effort. Statistical methods - correlation analysis - have been used on a large amount whereas significant correlations have been found between cloud fraction and precipitation, air temperature, and topography (Didier 2015, and Forsythe et al. 2015). With the recent rise of machine learning and availability of data, different studies showed a large correlation between cloud fraction and longwave radiation while estimating the downward longwave as mentioned in Dürr and Philipona 2004, the downward longwave at the surface is strongly influenced by the presence of cloud.

Machine learning techniques have been widely used in atmospheric radiative transfer studies due to its ability to address nonlinear complexity problems. In cloud-resolving models (CRMs), neural networks-based cumulus parameterization accurately diagnosed both precipitation and cloud fraction with little instability for multiple time steps prediction (Brenowitz and Bretherton 2018). By learning from CRMs simulations, deep neural networks achieved an accurate convection and rapid execution on accelerators like Graphical Processing Units (GPUs) (Ukkonen et al. 2020. Statistically, (Y. Cao, Li, and Zhang 2022) - with random forests (RF), extremely randomised trees (ERT), and categorical boosting (CatBoost) - found a high dependence of atmospheric temperature and water vapour on the Clear-sky longwave downward radiation. While estimating daytime downward longwave radiation under both cloudy and clear skies, (Carmona, Rivas, and Caselles 2014) with multiple linear regression found a high correlation between cloud fraction and longwave. Several studies have been done estimating longwave with cloud fractions as input, but no work done yet the other way around.

In this paper, with the use of the Reunion new station of the Baseline Surface Radiation Network (BSRN) recording climate parameters from June 2019, we achieved two major objectives. Cloud fraction estimation with use of machine learning model and NNs, XGBoost and ANN respectively. The use of XGBoost is based on its use of a tree and a sequential neural network, while ANN was used for comparison. In addition, a physical model was used to calculate cloud fraction from the parameters based on the physical relationship, and the two results were compared. Statistical metrics such as Mean Absolute Error (MAE), Root Mean Square Error (RMSE) and coefficient of correlation have been used to evaluate the results, and comparison of the longwave data with Clouds and the Earth's Radiant Energy System (CERES) data. And to evaluate the machine learning models, learning curves were used.

1 Data and methods

1.1 Datasets

Data wrangling and data quality control are vitally important step before studying and analysing data. Many data sources can be used as a reference for the validation. However, due to the availability of the data in terms of spatial resolution and temporal resolution, we chose CERES.

1.1.1 BSRN Reunion Moufia

The data from BSRN station benefit from automatic quality control and visual quality control (Long and Shi 2008). In addition, high precision sensors are used in all BSRN stations over the globe, calibrated every two years at the World Radiometric Reference and the World Radiation Centre (PMOD/WRC) in Davos.

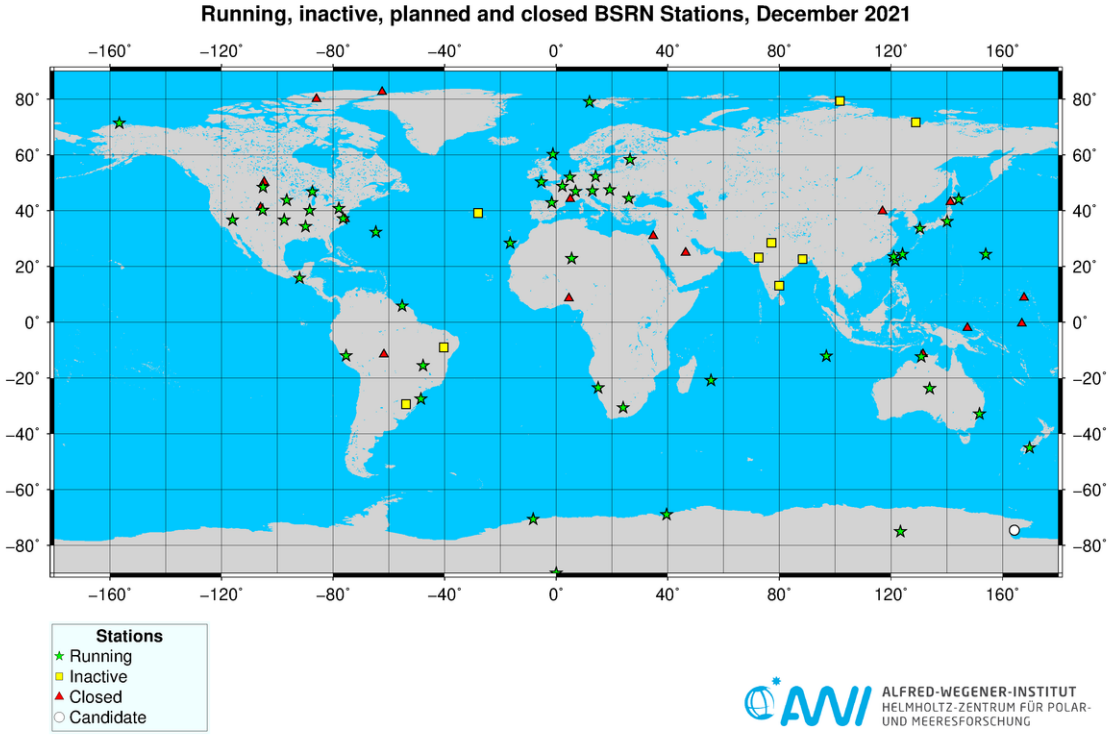

Figure 1: BSRN stations in the world

Even though the above make the data of a high quality, to ensure data quality from the Moufia BSRN station, CERES data were used for validation based on its availability and reference study done while validating BSRN Gobabeb (paper for cobabeb). Specifically, the one degree hourly Surface Fluxes - Longwave Flux -Down and Downward longwave from CERES were used to validate our BSRN longwave (citing the data).

Table 1: Measurements of BSRN Moufia station

Parameters	Units
Global shortwave	W/m2
Shortwave diffuse	W/m2
Shortwave direct	W/m2
Downward longwave	W/m2
Temperature	°C
Relative humidity	-
Pressure	Pa

After computing the mean absolute error (MAE) (Jia, N. Cao, and Yang 2021), root mean square error

(RMSE), and correlation coefficients (Jia, N. Cao, and Yang 2021, Jia, N. Cao, and Yang 2021), comparison was done with three different temporal resolutions: hourly, daily and monthly, and results are presented in the table or figure (cite the table).

The figure 2, 3 and 4 show a consistent smaller error over all temporal resolution, that corresponds to the use of updated high precision sensors from the PMOD/WRC. In addition, even though there is a decrease in error with increase in the resolution, it is faster on the BSRN Moufia than for Cobabeb . Again, BSRN Moufia data have comparable correlation with CERES as BSRN Cobabeb. The results are shown in figure 5,6 and 7. Irrespective of difference in locations and ages, BSRN Moufia data showed good accuracy to be used. The following Figures show the comparison ERA5 vs BSRN Reunion and Gobabeb vs CERES data :

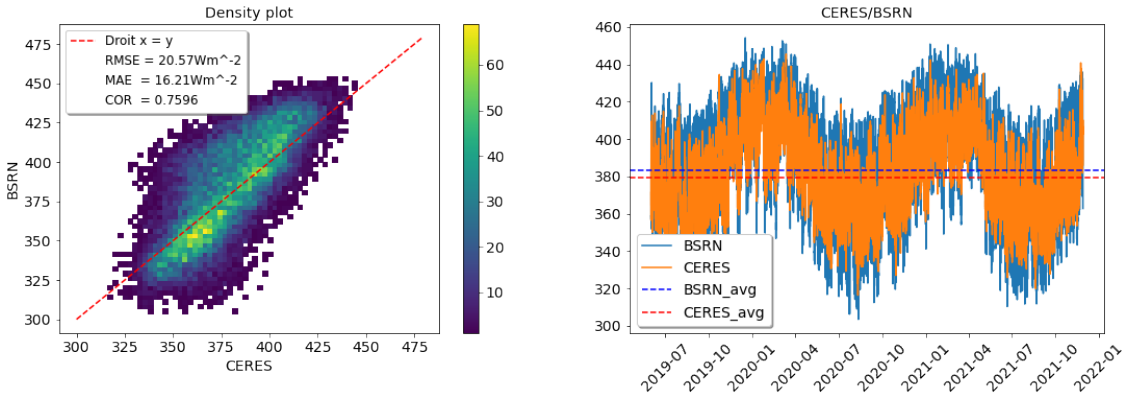

Figure 2: Ground measurement Reunion vs CERES hourly

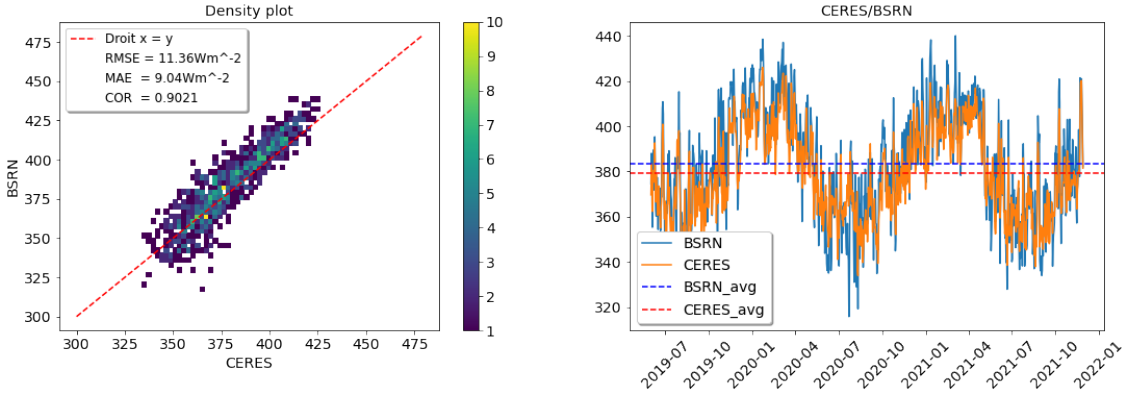

Figure 3: Ground measurement Reunion vs CERES daily

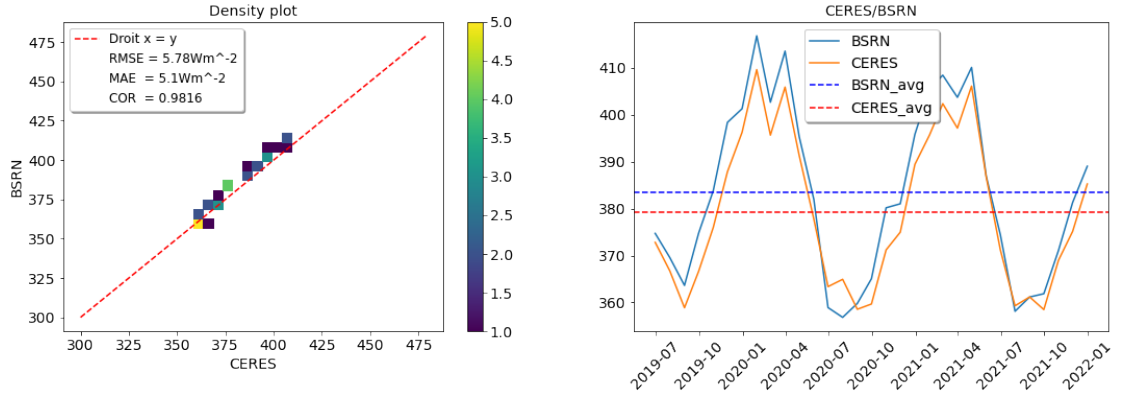

Figure 4: Ground measurement Reunion vs CERES monthly

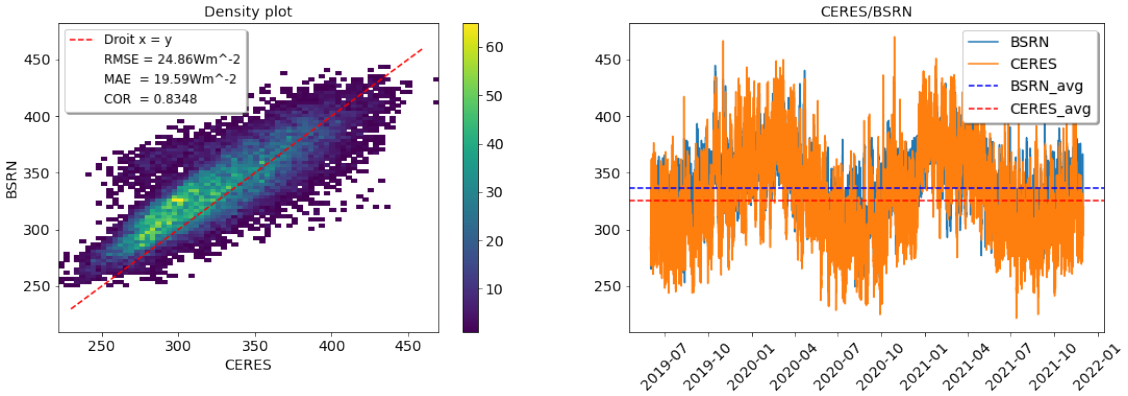

Figure 5: Ground measurement Gobabeb vs CERES hourly data

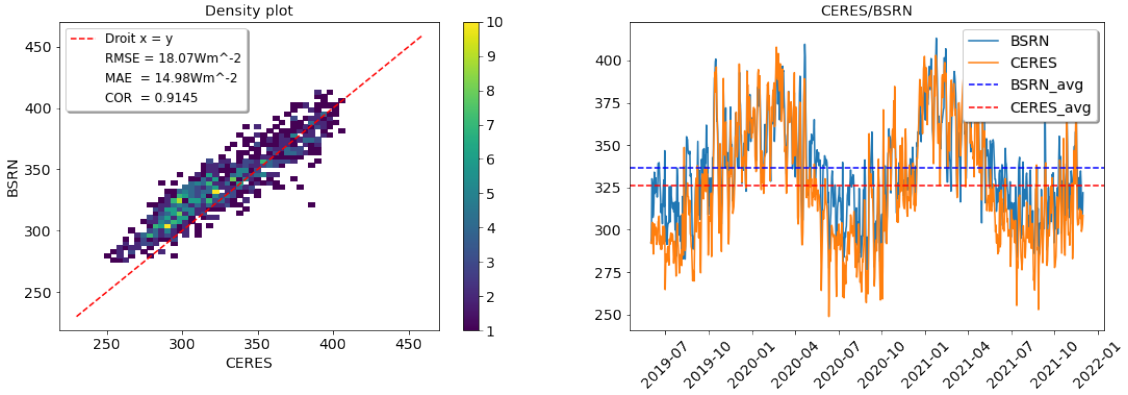

Figure 6: Ground measurement Gobabeb vs CERES daily data

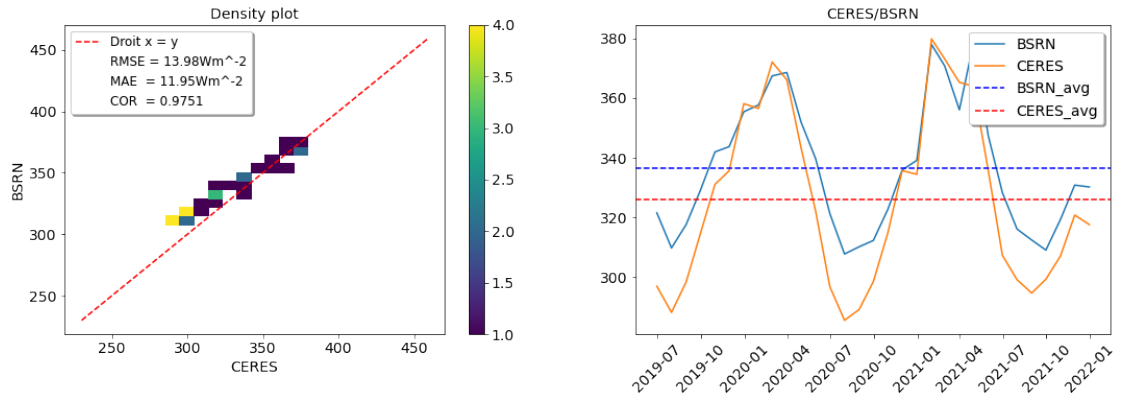

Figure 7: Ground measurement Gobabeb vs CERES monthly data

1.1.2 Longwave from Clouds and the Earth's Radiant Energy System (CERES)

The National Aeronautics and Space Administration's (NASA) Clouds and the Earth's Radiant Energy System (CERES) is included in the program for studying the earth from space using a multiple-instrument, multiple satellite approach (Wielicki et al. 1996). The mission is currently providing the climate community a 15-yr record of observed top-of-the-atmosphere (TOA) fluxes (Doelling et al. 2016) to examine the role of cloud and radiation feedback in the Earth's climate system (Wielicki et al. 1996). The CERES synoptic 1° (SYN1deg) product incorporates derived fluxes from the geostationary satellites (GEOs) to account for the regional diurnal flux variations in between Terra and Aqua CERES measurements. The data resolution temporal is available for 1-hour, 3-hour, daily and monthly. Different parameters can be downloaded from the site: `https://ceres.larc.nasa.gov/data/` (Synoptic TOA and surface fluxes and clouds (SYN)). In this study, the data from Surface Fluxes - Longwave Flux -Down are used with temporal resolution 1 hour.

1.1.3 Cloud fraction - longwave

Longwave measurement at the Earth surface is strongly influenced by clouds at different latitudes. With respect to the distance from the surface and altitude emittance temperature, effects of clouds decrease as clouds occupy higher altitude (**philipona2004greenhouse**). While evaluating influence of high clouds class on longwave downward radiation with radiative transfer model in MODerate resolution atmospheric TRANsmission (MODTRAN v4.0), effects were estimated to be 4 and 5 W/m2 for summer and winter respectively. Afterwards, studies focussed on lower altitude clouds in cloud effects quantification.

Through the Longwave variability we can separate broken cloud from cloud-free or overcast situations. Cloud-free and totally overcast situations are characterized by small Longwave variations. It can be demonstrated by comparing the Longwave Std with observed partial cloud amount (Dürr and Philipona 2004).

The Clear Sky Index is a powerful tool to detect clear-sky situations. Overall, it's intended to separate cloudy sky from cloudy-free situation with the data accurate longwave downward radiation and stadard meteorological air temperature and humidity measurement (Marty and Philipona 2000). The CSI is defined as :

$$CSI = \frac{\epsilon_A}{\epsilon_{AC}} \tag{1}$$

With :

- ϵ_A is the apparent emittance of the sky
- ϵ_{AC} is an empirical apparent cloud-free emittance

$$\epsilon_A = \frac{LDR}{\sigma_b T^4} \tag{2}$$

- LDR : Longwave Downward Radiation
- σ_b is the Stephan-Boltzmann constant
- T is the air temperature (K)

$$\epsilon_{AC} = \epsilon_{AD} + (k + 2\sigma)(\frac{e}{T})^{\frac{1}{8}} \tag{3}$$

- ϵ_{AD} : is an altitude-dependent emittance of a completely dry atmosphere
- e is water vapor pressure (Pa)
- k is a constant location-dependent coefficient

$$e = (\frac{RH}{100})e_S \tag{4}$$

- RH : Relative Humidity
- e_S is the empirical equation for the saturated water vapor pressure (in hPa)

$$e_S = 6.1121exp(\frac{17.502t_a}{t_a + 240.97}) \tag{5}$$

- t_a : air temperature t a has to be in °C.

CSI < or = 1 means cloud-free conditions, and CSI > 1 means cloudy sky. The CSI may also be divided in different subcategories to define the percentage of cloud coverage. With the dramatic decrease of uncertainty on longwave downward radiation measurements due to improved instruments and calibration techniques, the implementation of the CSI offers new possibilities in the field of meteorology and radiation climatology. Accurate and continuous determinations of cloud amount and cloud forcing from surface measurements are made possible with the Clear-Sky Index (Marty and Philipona 2000). Further investigations of cloud-free cases showed that high CSI values are correlated with negative vertical temperature gradients γ, ie, temperature inversions, near the surface during nighttime and daytime.

$$\gamma = -(\frac{\Delta T}{\Delta z}) \tag{6}$$

With : ΔT is the temperature difference over a vertical distance Δz around 30 m.

Thus variations of γ with time $\gamma(t)$ have to be considered for the calculation of CSI. The diurnal and annual cycle of $(\gamma(t))$ can be roughly approximated as a periodical function:

$$\gamma(t) = \gamma_0 + \gamma_{amp}\cos(wt - \frac{\pi}{4}) \tag{7}$$

with γ_0 the average

γ_{amp} the amplitude of γ

$\omega = 2/P$ with period P

We defined k equation (6) as a function of $\gamma(t)$ and accordingly replaced k by $k = k[\gamma(t)] = k(t)$:

$$k(t) = k_0 + k_{amp}\cos(wt - \frac{\pi}{4}) \tag{8}$$

with

$$k_0 = \frac{(k_{max} - k_{min})}{2} \tag{9}$$

and

$$k_{amp} = k_{max} - k_0 \tag{10}$$

Analogously, the constant confidence level 2 σ in equation (6) was replaced with a time-dependent shift function $\Delta k(t)$:

$$\Delta k(t) = \Delta k_0 + \Delta k_{amp}\cos(wt - \frac{\pi}{4}) \tag{11}$$

with

$$\Delta k_0 = \frac{\Delta k_{max} - \Delta k_{min})}{2} \tag{12}$$

and

$$\Delta k_{amp} = \Delta k_{max} - \Delta k_0 \tag{13}$$

The exponent value is set back to the original value of 1/7 (Brutsaert 1975) after evaluating fits of equation (6) to measured cloud-free emissivities at several radiation sites. Thus the apparent cloud-free emittance ϵ_{AC} in equation (6) is now formulated as:

$$\epsilon_{AC} = \epsilon_{AD} + (k(t) + \Delta k(\frac{e}{T})^{\frac{1}{7}} \tag{14}$$

The modified CSI using equation (17) is called the cloud-free index CFI:

$$CFI = \frac{\epsilon_A}{\epsilon_{AC}} \tag{15}$$

CFI < 1 or $= 1$ normally indicates cloud-free conditions, and CFI > 1 indicates cloudy sky. Determination of Site-Specific Functions like $k(t)$ and $\Delta k(t)$ are broken down in Dürr and Philipona 2004 for Annual Cycle and Diurnal Cycle. The measurement of partial cloud amount PCA is expressed in octa. A heuristic set of rules was developed to estimate PCA, this use CFI and Std of LDR. The algorithm called automatic partial cloud amount detection algorithm (APCADA).

1.1.4 Machine learning methods

Based on the study by Durr and Philipona (**philipona2004greenhouse**), estimating cloud fraction from longwave downward radiation, temperature, and relative humidity, machine learning techniques have been used. In addition, this study did not only consider the three variables, but also all measurements of BSRN Moufia (ref the table of BSRN parameters). Furthermore, the algorithm estimated cloud fraction every 5 minutes.

1.1.5 XGBoost model

The XGBoost algorithm belongs to the Gradient Boosting Decision Tree (GBDT) algorithm, which is an iterative decision tree algorithm consisting of multiple decision trees (citations). Starting with one weak learner, it iteratively adds new weak learners to approximate functional gradients (He et al. 2020). XGBoost provides a parallel tree boosting that solves data science problems in a fast and accurate way. Recently, XGBoost became one of the most popular Machine Learning algorithms based on the model accuracy, how it handles several kinds of data, and on the fact that mathematical tools are already embedded in the code libraries (citations). The table (ref) shows hyperparameters used to handle overfitting.

Table 2: XGBoost used hyper-parameters

Hyper-parameters	Values
N estimators	100
Learning rate	0.05
Max depth	6
Subsample	1
Colsample bylevel	0.8
Colsample bytree	1.0
Colsample bynodes	0.8
Min child weigth:	4

1.1.6 Artificial Neural Network

Artificial Neural network (ANNs) is a machine learning method capable of processing different forms of huge data - fuzzy, random, and nonlinear data - by learning tasks with a feed-forward multi-layer (nonlinear) network. Training process of ANNs usually consists of pre-training and fine-tuning (Kim and Lee 2016). To process the relationship between input and output, the network keeps adjusting the weight of neuron connections by repeatedly learning and training the data (**feng2020estimating**).

In this study, estimation of the cloud fraction with ANNs was implemented using python . . . ??. . . . . Among several methods, the technique from (citedomhan2015speeding) was used to optimise the hyper-parameters (why?). The table (ref) shows the predefined extent of the hyper-parameters.

Table 3: ANN used hyper-parameters

Hyper-parameters	Values
Number of hidden layers	100
Number of unit	10
Learning rate	0.007
Epoch	50
Batch size	10
Activation function	relu
Optimizer	Adam

1.1.7 Learning curve for diagnosing model

Learning curves are a widely used diagnostic tool in machine learning. *Learning curves are deemed effective tools for monitoring the performance of a model machine learning exposed to a new task. It provides a mathematical representation of the learning process that takes place as task repetition occurs* (Anzanello and Fogliatto 2011). Overall, it allows to evaluate the model during the training and validation.

- **Train Learning Curve**: Learning curve calculated from the training data set that gives an idea of how well the model is learning.
- **Validation Learning Curve**: Learning curve calculated from a holdout validation data set that gives an idea of how well the model is generalizing.

Both curves are necessary plotted on a single graph, it gives an idea of how well the model is learning. Several metrics can be used to evaluate the model : MAE, MSE, RMSE,... (**J.BrownleeLCs**).

2 Results and discussions

2.1 Estimation with XGBoost

In this section we are talking the performance of the model and the results. After training model, plotting learning curves is a mandatory to diagnose the model. Overall, during the training both curves are supposed to decrease together and the generalization gap between both curves is necessary low. Generalization gap is the difference between both curves. Three cases can be appears: over-fitting, under-fitting and good fitting. Over-fitting mean when the model is good during the training, but bad for the validation. Under-fitting mean the model doing great for the validation and bad for the training. Good fitting when the generalization gap is lower and both curves are nearly overlapping. The tuning hyper-parameters are necessary to solve over-fitting or under-fitting issues(**J.Brownlee**).
The following figure shows the learning curves before and after tuning hyper-parameters :

In the Figure 10, red curve represents the training curve and blue curve represent test or validation curve. Over-fitting is observed in the left Figure 10 because the model is not optimized. After tuning hyper-parameter, the generalization gap decrease and the accuracy, decrease shown in the right Figure 10. It is normal because after tuning hyper-parameters the model become less complex and generalized well the value estimated. We get more robustness after tuning model (validation score become 92.44 % instead 94.20 %) and the predicted result is more reliable. The following figure shows the prediction results :

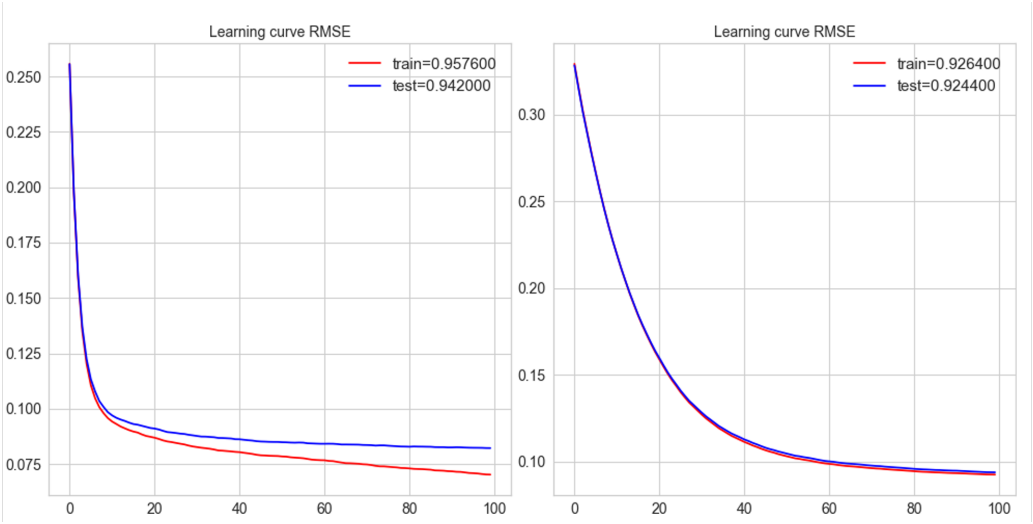

Figure 8: Learning curves before and after tuning hyper parameters

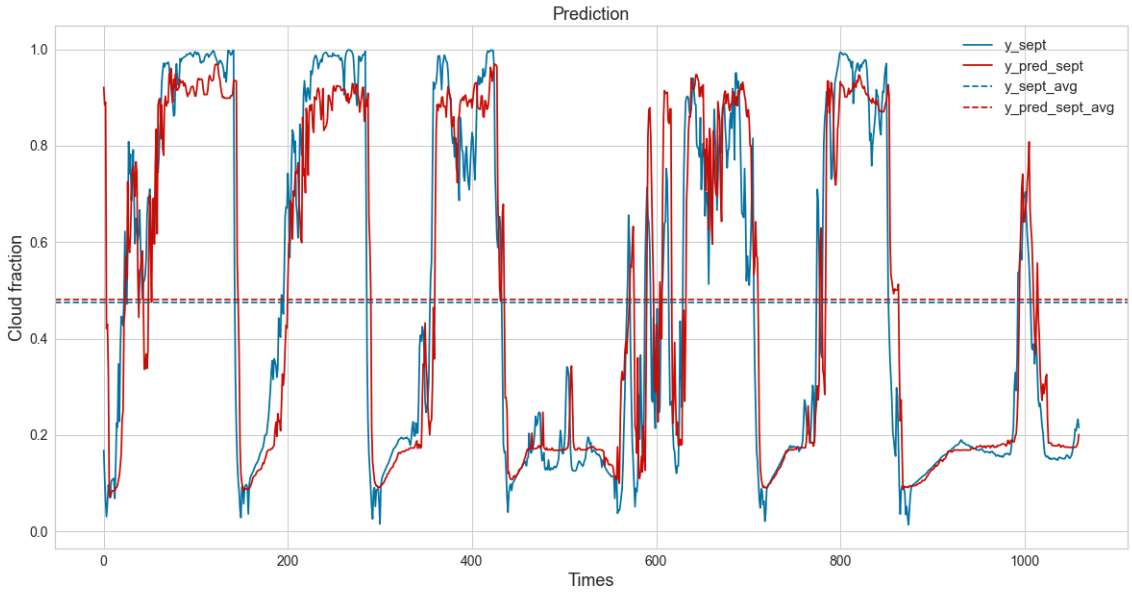

Figure 9: Estimation of cloud fraction with XGBoost model

In this Figure 11, red curve represents the predicted value of the model and blue curve is the real value measured. The data set used for train and validation start from 2019-09-13 to 2021-01-03. The data set prediction start from 2021-01-04 to 2021-02-01. The temporal resolution equal 5 min. We used data from 2021-02-02 to 2021-02-27 for the prediction. We remark some difference in amplitude, in the major part of the prediction, the model underestimates the maximum value, it is normal because the model is supposed to generalize the value predicted. We got a score 92.44 % for the model XGBoost.

To enhance the model, feature engineering was applied and several tests were realized. The results after feature elimination based on feature importance (Figure 12) are presented in the Figure 13. We tried six possibility combination features and the scores results are shown in the Table 4.

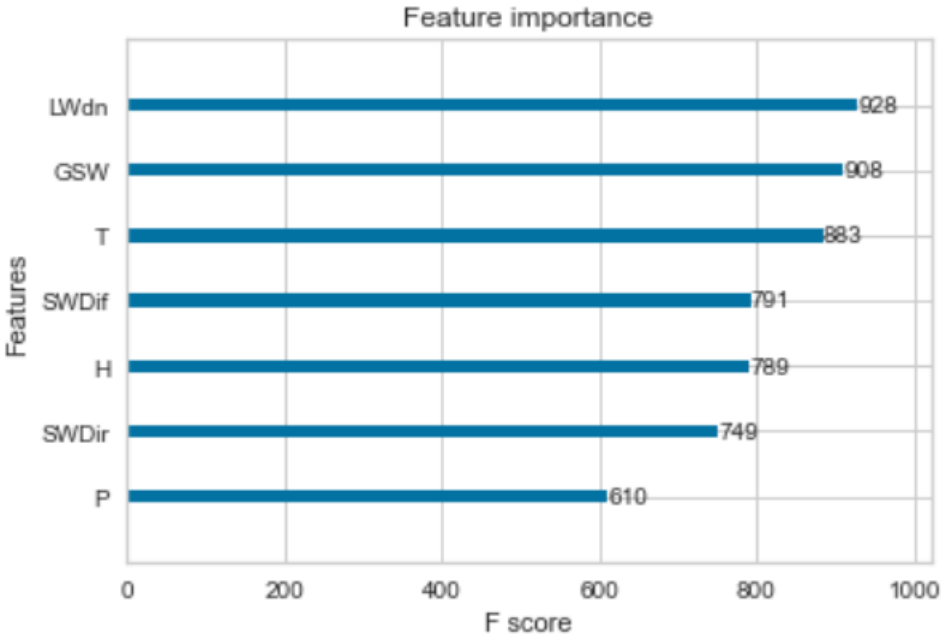

Figure 10: Features importance

The following table summarized the scores of each model:

Table 4: Validation score

Features	Train	Validation
LWdn, GSW, T, SWDif, RH, SWDir, P	92.45	92.23
LWdn, GSW, T, SWDif, RH, SWDir	92.21	92.02
LWdn, GSW, T, SWDif, RH	91.80	91.67
LWdn, GSW, T, SWDif	90.89	90.89
LWdn, GSW, T	87.35	87.31
LWdn, GSW	70.39	69.08

It is clear that when we reduce features number the precision decrease with and the model ends up underfitting as features are eliminated. For both first figures, the precision is piratically similar, The difference is within the features combination. The first model with complete input and the second model without pressure on input, and we get scores 92.23 % and 92.02 % respectively. The difference lies in the complexity of the model. The first model is more complex than the second, it's due to the presence of pressure feature which does not lead to much change within the model precision. Hence, the best model is the model with feature without pressure, because we have.

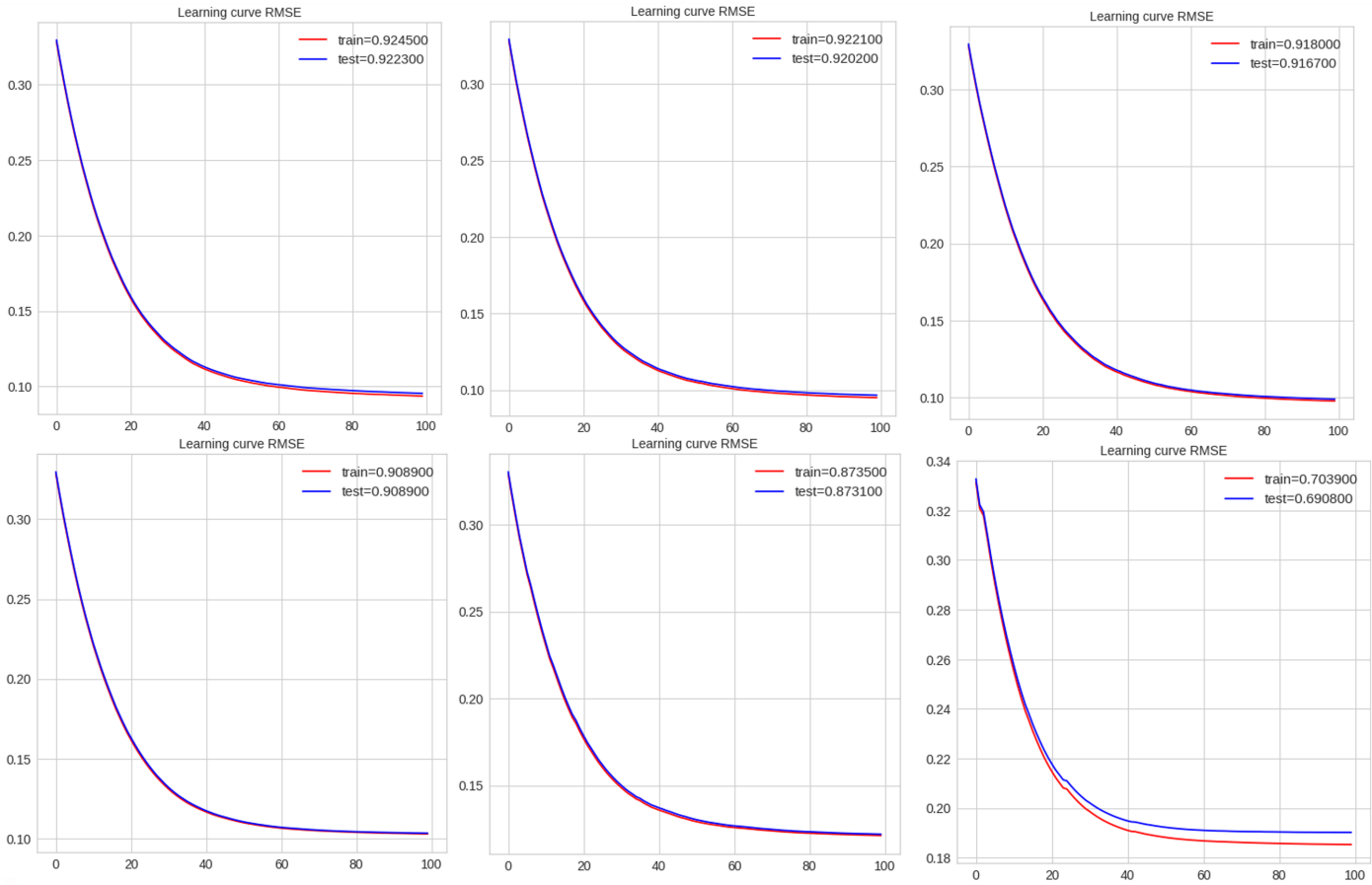

Figure 11: Learning curves with different features

2.2 Estimation with XGBoost

In the following figure, we have the results of the model sequential neural network:

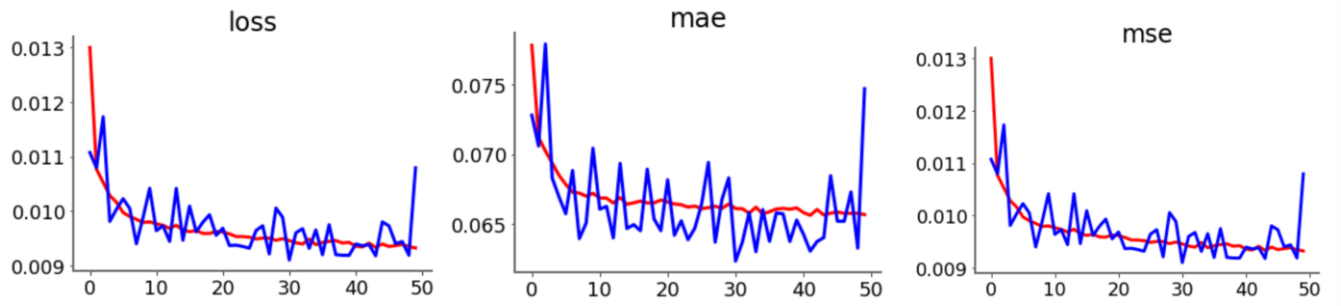

Figure 12: Loss function, MAE and MSE

The Figure 12 shows the three learning curves with loss MSE, MAE and MSE metrics. The blue curve represents the training curves and the orange curve represent the validation curves. Three metrics show us a good fit for the model. The prediction curves in the Figure 13 show also a good prediction with 91.78 % score. For a neural network this is a very good score. The next Figure show the prediction results with neural network:

Table 5: Metrics results for the model ANN

Features	loss	mae	mse
LWdn, GSW, T, SWDif, RH, SWDir, P	0.86 %	6.58 %	0.86 %

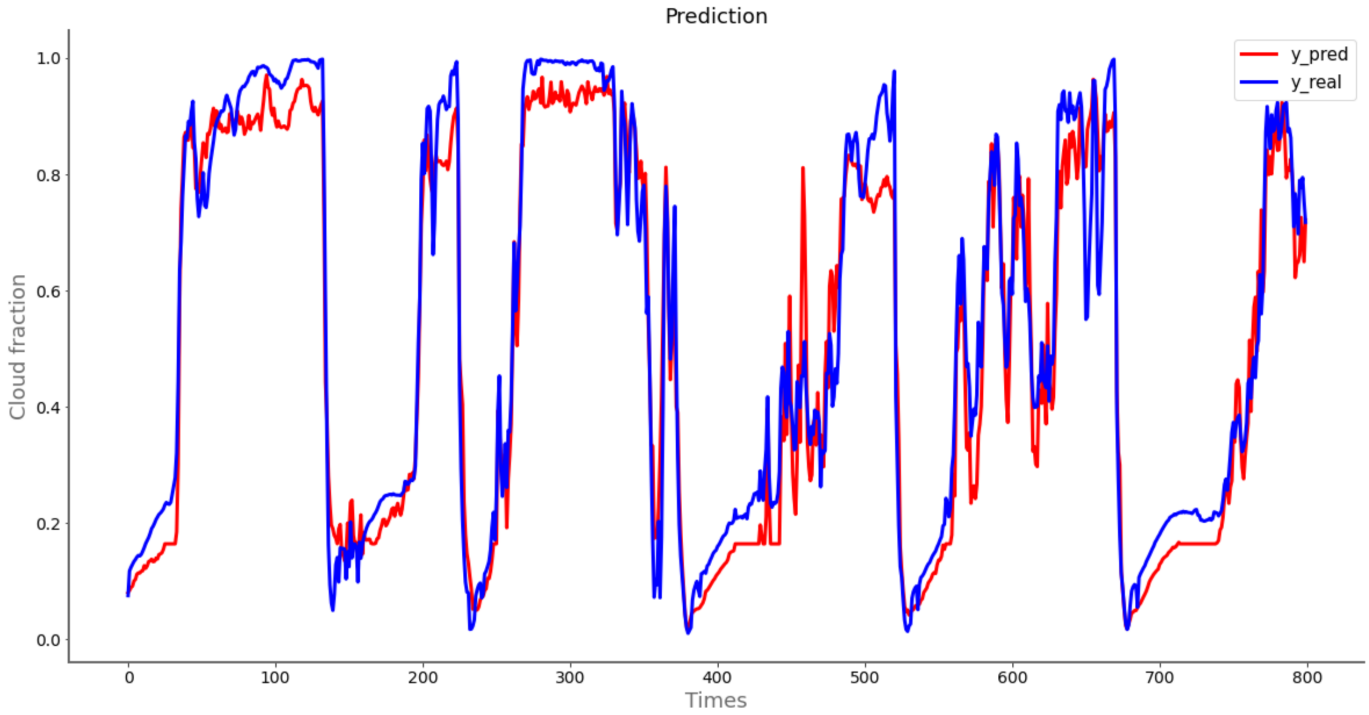

Figure 13: Estimation by neural network

Conclusions

In this paper, we got good results for both goals. The longwave data validation shows a difference within an amplitude due to the physical laws on the ground surface. However, we got good statistical results when we compare the values of RMSE and MAE with the results obtained in Jiao and Mu 2022 and Feng et al. 2021. The data validation can be realised whit other data reference source, but we are constrained by the availability of the data in term of temporal resolution and spatial resolution. Concerning the results about cloud fraction estimation using XGBoost model and ANN model, the results demonstrate a good performance of XGBoost and ability to estimate the cloud fraction. The performance of XGBoost is evaluated by error analysis indicators such as R2, RMSE and MAE. For XGBoost model we had a score 92.21 % , it is a good results comparable to the results in the Han et al. 2019 and Ma, Fang, and Ji 2020. For the ANN model, it performed better with the score 91.78 % a lower value for MAE and MSE are obtained by comparing to the results from Dhakal, Gautam, and Bhattarai 2020 after optimizing the model ANN.

There are a lot of machine learning model and neural network model can be used for this kind of problem. The comparison of the results from these models allows us to find the best model after tuning each model. Adding data set and features are also very important for the model. Adding new features like an aerosol can be lead more precision for the model machine learning, cloud fraction and aerosol have a strong correlation (Gryspeerdt, Quaas, and Bellouin 2016). The other features candidate needs an investigation of the link between the target and the new features.

Acknowledgment

References

Brutsaert, Wilfried (1975). "On a derivable formula for long-wave radiation from clear skies". In: *Water resources research* 11.5, pp. 742–744.

Aida, Masaru (1977). "Reflection of solar radiation from an array of cumuli". In: *Journal of the Meteorological Society of Japan. Ser. II* 55.2, pp. 174–181.

Ellingson, Robert G (1982). "On the effects of cumulus dimensions on longwave irradiance and heating rate calculations". In: *Journal of Atmospheric Sciences* 39.4, pp. 886–896.

Heidinger, Andrew K and Stephen K Cox (1996). "Finite-cloud effects in longwave radiative transfer". In: *Journal of Atmospheric Sciences* 53.7, pp. 953–963.

Wielicki, Bruce A et al. (1996). "Clouds and the Earth's Radiant Energy System (CERES): An earth observing system experiment". In: *Bulletin of the American Meteorological Society* 77.5, pp. 853–868.

Marty, Christoph and Rolf Philipona (2000). "The clear-sky index to separate clear-sky from cloudy-sky situations in climate research". In: *Geophysical Research Letters* 27.17, pp. 2649–2652.

Dürr, Bruno and Rolf Philipona (2004). "Automatic cloud amount detection by surface longwave downward radiation measurements". In: *Journal of Geophysical Research: Atmospheres* 109.D5.

Long, Chuck N and Yan Shi (2008). "An automated quality assessment and control algorithm for surface radiation measurements". In: *The Open Atmospheric Science Journal* 2.1.

Anzanello, Michel Jose and Flavio Sanson Fogliatto (2011). "Learning curve models and applications: Literature review and research directions". In: *International Journal of Industrial Ergonomics* 41.5, pp. 573–583.

Carmona, Facundo, Raúl Rivas, and Vicente Caselles (2014). "Estimation of daytime downward longwave radiation under clear and cloudy skies conditions over a sub-humid region". In: *Theoretical and applied climatology* 115.1, pp. 281–295.

Didier, Ntwali (2015). "Comparison of spatial and temporal cloud coverage derived from CloudSat, CERES, ISCCP and their relationship with precipitation over Africa". In: *American Journal of Remote Sensing* 3.2, pp. 17–28.

Forsythe, N et al. (2015). "A detailed cloud fraction climatology of the Upper Indus Basin and its implications for near-surface air temperature". In: *Journal of climate* 28.9, pp. 3537–3556.

Doelling, David R et al. (2016). "Advances in geostationary-derived longwave fluxes for the CERES synoptic (SYN1deg) product". In: *Journal of Atmospheric and Oceanic Technology* 33.3, pp. 503–521.

Gryspeerdt, Edward, Johannes Quaas, and Nicolas Bellouin (2016). "Constraining the aerosol influence on cloud fraction". In: *Journal of Geophysical Research: Atmospheres* 121.7, pp. 3566–3583.

Brenowitz, Noah D and Christopher S Bretherton (2018). "Prognostic validation of a neural network unified physics parameterization". In: *Geophysical Research Letters* 45.12, pp. 6289–6298.

Han, Yixiu et al. (2019). "Coupling a bat algorithm with xgboost to estimate reference evapotranspiration in the arid and semiarid regions of china". In: *Advances in Meteorology* 2019.

Dhakal, Sandeep, Yogesh Gautam, and Aayush Bhattarai (2020). "Evaluation of temperature-based empirical models and machine learning techniques to estimate daily global solar radiation at Biratnagar Airport, Nepal". In: *Advances in Meteorology* 2020.

Ma, Xiaoming, Cong Fang, and Junping Ji (2020). "Prediction of outdoor air temperature and humidity using Xgboost". In: *IOP Conference Series: Earth and Environmental Science*. Vol. 427. 1. IOP Publishing, p. 012013.

Ukkonen, Peter et al. (2020). "Accelerating radiation computations for dynamical models with targeted machine learning and code optimization". In: *Journal of Advances in Modeling Earth Systems* 12.12, e2020MS002226.

Feng, Chunjie et al. (2021). "Estimation of Long-Term Surface Downward Longwave Radiation over the Global Land from 2000 to 2018". In: *Remote Sensing* 13.9, p. 1848.

Jia, Pengcheng, Nianwen Cao, and Shaobo Yang (2021). "Real-time hourly ozone prediction system for Yangtze River Delta area using attention based on a sequence to sequence model". In: *Atmospheric Environment* 244, p. 117917.

Cao, Yunfeng, Manyao Li, and Yuzhen Zhang (2022). "Estimating the Clear-Sky Longwave Downward Radiation in the Arctic from FengYun-3D MERSI-2 Data". In: *Remote Sensing* 14.3, p. 606.

Jiao, Zhong-Hu and Xihan Mu (2022). "Global validation of clear-sky models for retrieving land-surface downward longwave radiation from MODIS data". In: *Remote Sensing of Environment* 271, p. 112903.